remote sensing

MDPI

Article

Application of a Multispectral UAS to Assess the Cover and Biomass of the Invasive Dune Species *Carpobrotus edulis*

Manuel de Figueiredo Meyer [1], José Alberto Gonçalves [1,2], Jacinto Fernando Ribeiro Cunha [1,3], Sandra Cristina da Costa e Silva Ramos [1] and Ana Maria Ferreira Bio [1,*]

[1] Interdisciplinary Centre of Marine and Environmental Research (CIIMAR/CIMAR), University of Porto, 4099-002 Porto, Portugal; mmeyer@ciimar.up.pt (M.d.F.M.)
[2] Department of Geosciences Environment and Spatial Planning, Faculty of Sciences, University of Porto, 4169-007 Porto, Portugal
[3] Centre for the Research and Technology of Agro-Environmental and Biological Sciences (CITAB), University of Trás-os-Montes and Alto Douro, 5000-801 Vila Real, Portugal
* Correspondence: anabio@ciimar.up.pt

Abstract: Remote sensing can support dune ecosystem conservation. Unoccupied Aircraft Systems (UAS) equipped with multispectral cameras can provide information for identifying different vegetation species, including *Carpobrotus edulis*—one of the most prominent alien species in Portuguese dune ecosystems. This work investigates the use of multispectral UAS for *C. edulis* identification and biomass estimation. A UAS with a five-band multispectral camera was used to capture images from the sand dunes of the Cávado River spit. Simultaneously, field samples of *C. edulis* were collected for laboratorial quantification of biomass through Dry Weight (DW). Five supervised classification algorithms were tested to estimate the total area of *C. edulis*, with the Random Forest algorithm achieving the best results (*C. edulis* Producer Accuracy (PA) = 0.91, *C. edulis* User Accuracy (UA) = 0.80, kappa = 0.87, Overall Accuracy (OA) = 0.89). Sixteen vegetation indices (VIs) were assessed to estimate the Above-Ground Biomass (AGB) of *C. edulis*, using three regression models to correlate the sample areas VI and DW. An exponential regression model of the Renormalized Difference Vegetation Index (RDVI) presented the best fit for *C. edulis* DW (R^2 = 0.86; *p*-value < 0.05; normalised root mean square error (NRMSE) = 0.09). This result was later used to estimate the total AGB in the area, which can be used for monitoring and management plans—namely, removal campaigns.

Keywords: multispectral images; unoccupied aircraft systems; invasive species; vegetation indices; above-ground biomass; QGIS

Citation: Meyer, M.d.F.; Gonçalves, J.A.; Cunha, J.F.R.; Ramos, S.C.d.C.e.S.; Bio, A.M.F. Application of a Multispectral UAS to Assess the Cover and Biomass of the Invasive Dune Species *Carpobrotus edulis*. *Remote Sens.* **2023**, *15*, 2411. https://doi.org/10.3390/rs15092411

Academic Editors: Evangelos Alevizos and Konstantinos Topouzelis

Received: 8 February 2023
Revised: 28 April 2023
Accepted: 2 May 2023
Published: 4 May 2023

1. Introduction

Coastal sand dunes constitute a vital ecosystem that provides multiple ecosystem services, including coastal protection against erosion, wind and wave impacts, reduction of overtopping and flood risks, recycling nutrients, recreation, and the filtration, retention, and storage of freshwater [1]. The integrity of this ecosystem is intrinsically connected with vegetation [2], as the plants' roots help stabilise the dunes and the aerial parts act as a wind barrier capturing and retaining sediments, reducing wave and wind-driven erosion [3]. Coastal dune environments also contribute to improving biodiversity by hosting different habitats and species [4].

Nevertheless, dune ecosystems face numerous threats, with dune vegetation being especially sensitive to disturbance and heavily affected by humans. Along with the degradation of dunes due to urbanisation and infrastructures or careless visitors, these ecosystems are highly susceptible to invasive plant species that compete with native species [5]. As autochthonous dune vegetation is damaged or removed, invasive species get a chance to expand their distribution area [6], leading to biodiversity loss.

A prominent alien species in European, and particularly in Northern-Portuguese dunes, is the ice plant *Carpobrotus edulis* [6]. This perennial creeping subshrub was initially introduced from South Africa as an ornamental plant and later used for slope stabilisation [1], but is now considered an important invasive species that threatens local dune vegetation and demands attention and monitoring to preserve sensitive dune ecosystems. *C. edulis* is characterised by fleshy leaves and large pink or yellow flowers. This species typically shows two layers: the green upper layer, which absorbs and reflects the sunlight, has succulent leaves and wet parts, and the lower layer is composed of older brown and dry leaves. The species directly competes with native plants for water, space, and sunlight, reducing and suppressing their growth and reproduction [7,8]. In addition, the dead matter of *C. edulis* can affect the soil's physicochemical and biological parameters, adding more carbon to the substrate and possibly altering the germination and physiology of native species [7,9].

In the past ten years, the use of Unoccupied Aircraft Systems (UAS) for ecosystem monitoring has become increasingly frequent, driven by the miniaturisation and development of cameras, sensors, and positioning systems, which allow the collection of high-resolution and precision imagery at a low cost. Being relatively cheap and easy to deploy, UAS carrying RGB, multi-, or hyper-spectral cameras have become a useful tool—especially for monitoring highly dynamic ecosystems at a local scale [10]. Multispectral UAS has been particularly widely disseminated in agriculture to assess within-field crop growth conditions [11]. Previous studies have indicated that Vegetation Indices (Vis) obtained from multispectral images can estimate plant biomass with satisfactory precision for commercial crop cultures [12,13]. In recent years, different equipment carrying multispectral cameras has also had an essential role in identifying and monitoring alien species-invaded areas [14–18]. The correlations of VIs and quantifiable vegetation parameters of invasive species have also been assessed, presenting different results depending on the species, methodology, equipment, and resolution. [19–21].

The main objective of this work was to develop and test a UAS remote-sensing methodology for (i) identification of the invasive species *C. edulis* based on its multispectral signature, and (ii) determination of the *C. edulis* cover area and biomass in the sandy dunes of a Marine Protected Area of NW Portugal (PNLN—Parque Natural do Litoral Norte). The results of this work can support the management of invasive species in dunes, providing an affordable method for the monitoring and quantification of *C. edulis*.

2. Materials and Methods

This study of *C. edulis* cover and biomass was based on the species' spectral signature in multispectral imagery and on the relationship between the species' biomass and VIs. After the presentation of the study area (Section 2.1), the procedures are presented divided into three phases: in situ work—including fieldwork and remote sensing (Section 2.2)—laboratory work for biomass estimation (Section 2.3), and image and biomass analyses (Section 2.4). The workflow is summarised in Figure 1.

2.1. Study Area

The study area is located on the northern coast of Portugal, on the estuarine sandspit of the river Cávado, the largest watershed of the PNLN—a marine protected area on the Northern Atlantic Coast of Portugal. The PNLN occupies a coastal stretch of about 16 km between the Neiva estuary (41°36′46.56″N, 8°48′32.55″O) and the southern border of Apúlia (41°28′10.68″N, 8°46′31.30″O), extending its area 5 km into the sea (Figure 2). Covering a total area of 8887 ha—of which 7653 ha are marine areas—it is administered by the Portuguese nature and forest conservation institute (Instituto da Conservação da Natureza e das Florestas—ICNF).

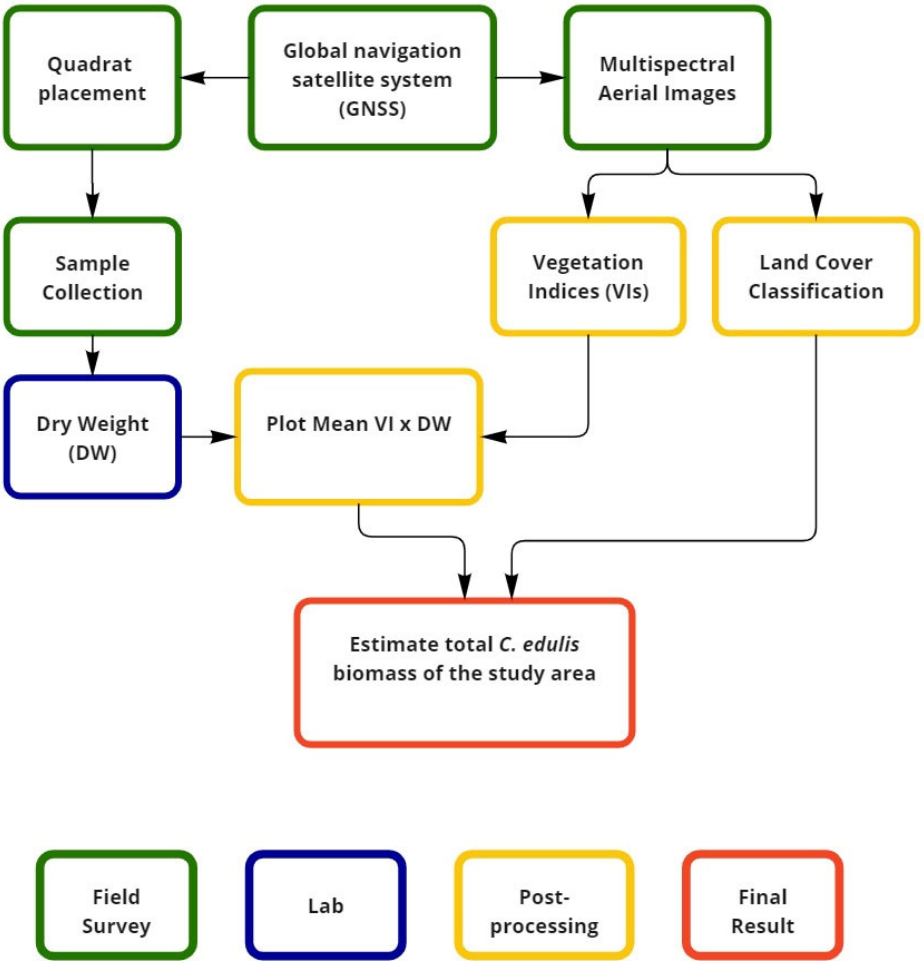

Figure 1. Workflow used to estimate *C. edulis* biomass in sand dunes.

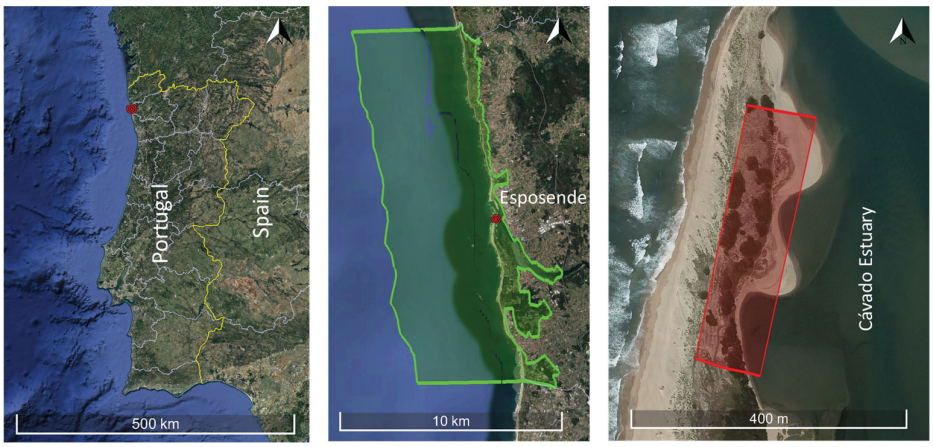

(**a**) (**b**) (**c**)

Figure 2. Location of the study area (red) in northern Portugal (**a**), within the Northern Littoral Natural Park ((**b**) park area in green) and on the estuarine sandspit (**c**) (Image: Google Earth—SIO, NOAA, U.S. Navy, NGA, GEBCO).

The PNLN was created to protect the littoral of Esposende, preserve its natural resources and elements, and promote the rational and sustainable use of the area. With its mainland consisting essentially of a strip of sandy shores, it houses 15 different habitats described in the Habitat Directive, with four of them marked as priority habitats: 1150—Coastal lagoons, 2130—Fixed coastal dunes with herbaceous vegetation (grey dunes), 2270—Wooded dunes

with *Pinus pinea* and/or *Pinus pinaster*, and 91E0—Alluvial forests with *Alnus glutinosa* and *Fraxinus excelsior* (*Alno-Padion*, *Alnion incanae*, *Salicion albae*).

There are 240 different vegetation species identified on the NLNP, with most of them native to the north Iberian littoral—including some endangered species; this native vegetation is vital for preserving its morphological and biotic characteristics [22]. Twelve invasive vegetation species were identified within the flora, the most prominent being *Acacia longifolia* and *Carpobrotus edulis,* which pose significant pressure on the dunar habitats [7]. Studying and monitoring the invasive species in the park can play a crucial role in preserving the NLNP habitats.

Almost all the in-land park area has an altitude of less than 10 m above mean sea level, with only some dunes with heights between 10 and 20 m. Like many other coastal environments, the park dunes suffer not only from invasive species but also from erosion risks, which are expected to increase due to climate change and pressures related to urbanisation and recreation (trampling) [23].

2.2. Survey and Fieldwork

The study area was surveyed in May 2022 with two UAS—one with a multispectral camera for the study of *C. edulis*, and a second one with a higher-resolution RGB camera to facilitate the identification of land cover for the classification process. Multispectral images were taken with a DJI M200 equipped with a MicaSense RedEdge-MX multispectral camera (Table 1) flying at 30 m height, which resulted in 5135 images with a 2.5 cm Ground Sample Distance (GSD). RGB images were taken with the inbuilt camera of a PHANTOM 4DJI flying at 30 m height, providing 136 images with a GSD of 1.0 cm.

Table 1. MicaSense RedEdge-MX Band specifications.

Band	Centre Wavelength	Bandwidth
Blue	475 nm	32 nm
Green	560 nm	27 nm
Red	668 nm	16 nm
Red Edge	717 nm	12 nm
Near Infrared	842nm	57 nm

Prior to the flights, thirty 50 × 50 cm^2 quadrats were placed over *C. edulis* vegetation with different densities and health conditions to obtain information about a range of densities and biomasses (Figure 3). The quadrats were placed in a North–South orientation to maximise the number of useful image pixels within the frame and to reduce the interference of the frame in the images, as flights and image pixels were also North–South oriented. All quadrats were placed in areas containing only *C. edulis* to obtain the best possible spectral signatures for the target species.

After the flights, the whole Above-Ground Biomass (AGB) of *C. edulis* within the central 30 × 30 cm^2 of each quadrat (Figure 3b) was removed, bagged, and tagged, and taken to the lab for biomass determination. This way, only the biomass corresponding to the image pixels unaffected by the frame was considered, as the sunlight reflection of the quadrat may interfere with the reflectance of *C. edulis*—especially on the boundary between the quadrat and the vegetation (as shown in a previous test survey).

The quadrats were georeferenced with a dual-frequency differential high-precision Global Navigation Satellite System (GNSS) antenna (NovAtel GPS-702-GG) in Real Time Kinematic (RTK) mode with fixed-station corrections using the RENEP network. These quadrats also served as Ground Control Points (GCP), placed next to 8 additional equally georeferenced GCP to enhance orthomosaic geometry and geolocation precision during imagery processing (Section 2.4).

(**a**) (**b**) (**c**)

Figure 3. Fieldwork: placement of a quadrat on a *C. edulis* patch (**a**), with other vegetation covers visible to the left (various herbaceous species) and in the back (acacia), delimitation of the central 30 × 30 cm^2 area within a quadrat for AGB removal (**b**), and the lower layer of brown parts of *C. edulis* exposed after removal of the upper green layer (**c**).

2.3. Laboratory Work

In the lab, the *C. edulis* AGB collected in each sample quadrat was processed to separate the upper green and succulent layer—which absorbs and reflects the sunlight and is visible in the aerial images—from the lower layer, composed of much dryer parts with older brown and dry leaves that are not visible in the aerial images. Then, each sample's green and brown parts were labelled and weighed (to the nearest 0.01 g), to obtain the upper- and lower-layer's wet weight (WW), and subsequently dried for seven days at 60 °C to a constant weight to obtain both layers' Dry Weight (DW).

These weight measurements were used to (i) assess the biomass ratio between the green and brown parts of the plants—necessary for estimating the total biomass, (ii) compare the DW and WW, and (iii) relate biomass with VIs (Section 2.4).

2.4. Image and Biomass Analyses

Multispectral and RGB orthomosaics were built using Agisoft Metashape Professional (version 1.8.3). The higher-resolution RGB ortho was only used to visually evaluate the land cover. The multispectral ortho was used to obtain VIs, which will be used later to assess their correlation with the measured DWs.

Maps of 16 previously evaluated VIs [13] (Table 2) were computed in QGIS (version 3.22.7) and the mean VI value was determined for the pixels of each 30 × 30 cm^2 sample area.

Table 2. Vegetation indices formulas used in this work.

Index	Formula	References
Atmospherically Resistant Vegetation Index (ARVI)	$\frac{NIR-(Red-Blu)}{NIR+(Red-Blu)}$	[24]
Green Chlorophyll Index (GCI)	$\frac{NIR}{Red}-1$	[25]
Chlorophyll Vegetation Index (CVI)	$\frac{NIR\times Red}{Gre^2}$	[26]
Difference Vegetation Index (DVI)	$NIR-Red$	[27]
Green Difference Vegetation Index (GDVI)	$NIR-Gre$	*
Enhanced Normalized Difference Vegetation Index (ENDVI)	$\frac{(NIR-Gre)-2Red}{(NIR-Gre)+2Red}$	[28]
Excess Green (ExG)	$2Gre-Red-Blu$	[29]
Excess Red (ExR)	$1.4Red-Gre$	[30]
Green Normalized Difference Vegetation Index (GNDVI)	$\frac{NIR-Gre}{NIR+Gre}$	[31]
Modified Green Red Vegetation Index (MGRVI)	$\frac{Gre^2-Red^2}{Gre^2+Red^2}$	[32]

Table 2. *Cont.*

Index	Formula	References
Normalized Difference Red Edge Index (NDREI)	$\frac{NIR-RDG}{NIR+RDG}$	[33]
Normalized Difference Vegetation Index (NDVI)	$\frac{NIR-Red}{NIR+Red}$	[29]
Photochemical Reflectance Index (PRI)	$\frac{Gre-Blu}{Gre+Blu}$	[34]
Red–Blue difference (RB)	$Red - Blu$	*
Renormalized Difference Vegetation Index (RDVI)	$\frac{NIR-Red}{\sqrt{NIR+Red}}$	[35]
Ratio Vegetation Index (RVI)	$\frac{Red}{NIR}$	[36]

Bands: Blu—Blue; Gre—Green; RDG—Red Edge; NIR—Near Infrared. * Experimental Indices tested in this study.

The mean VI values of each of the thirty 30 × 30 cm^2 samples were subsequently plotted against the DW values of the green parts of the plants (because the multispectral images capture only the reflectance of the top layer of *C. edulis*). The following models for estimating the DW from the different VIs were fitted and evaluated based on their R^2 and *p*-value:

$$\text{Linear model (lin)} \; y = a + bx$$

$$\text{Exponential model 1 (xpo1)} \; y = ab^x$$

$$\text{Exponential model 2 (xpo2)} \; y = ae^{xb}$$

where:

y = Dry Weight (DW);
x = Vegetation Index (VI);
a = coefficient 1;
b = coefficient 2.

To evaluate the total area of *C. edulis* cover, different supervised classification procedures were executed with the multispectral orthomosaic, using five algorithms: Minimum Distance [37], Maximum Likelihood [37], Spectral Angle Mapper [38], Support Vector Machines [39], and Random Forest [40]. The number of cover classes for the classifications was determined by visual identification of the most relevant cover types in the study area, and thirty Regions of Interest (ROI) were created for each class (Figure 4c). It is important to state that, in a first approach, the AGB sample areas were used as *C. edulis* classification training areas, but this did not lead to good classification results for two reasons: (i) the spectral signature of the areas had a high Standard Deviation, which made it hard to differentiate *C. edulis* from green vegetation and (ii) some of the sample areas presented very sparse vegetation, which was intentional, as sampling was designed to include samples for the lower end of the AGB x VI regression. This approach was later discarded, and thirty homogeneous ROIs were created close to the sample areas, with visual identification support.

Classification accuracy was assessed based on a large set of randomly selected pixels, for which the ground truth class was visually identified in the high-resolution RGB orthomosaic. Validation pixels were then compared with the supervised classification class, computing an error matrix for each classification. The number of pixels for the random-pixel accuracy test was defined based on the proportion of each class and the expected standard deviation of each class [41] according to the following equation:

$$N = \left(\sum_{i=1}^{6} (W_i S_i) / S_0\right)^2 \quad (1)$$

where:

N = Number total number of pixels;
W_i = mapped area proportion of class I;
S_i = standard deviation of stratum I;
S_0 = expected standard deviation of overall accuracy.

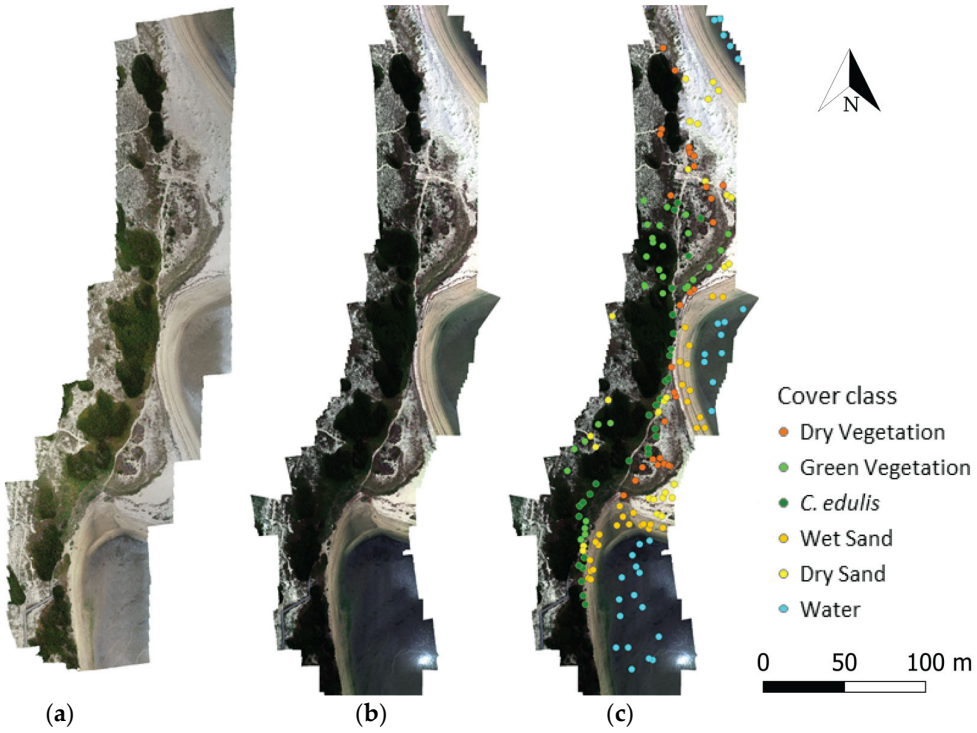

Figure 4. Orthomosaics of the RGB (**a**) and multispectral (**b**) images, and multispectral images with the location of the classification training and validation areas (**c**).

The different classifications were evaluated in terms of overall accuracy (OA), calculated by dividing the total number of correctly classified pixels by the total number of selected pixels; the Kappa statistic, which measures the agreement between classification and ground truth pixels—where Kappa = 1 means a perfect agreement while Kappa = 0 means a random agreement; the User Accuracy (UA) for the *C. edulis* class, calculated by dividing the number of correctly classified *C. edulis* pixels by the total number of pixels classified as *C. edulis*; and the Producer Accuracy (PA) for the *C. edulis* class, calculated by dividing the number of correctly classified *C. edulis* pixels by the number of pixels known to be of *C. edulis*.

A post-classification procedure was then performed to reduce the existence of small erroneously classified pixels by using two sieve filters of progressive strength to reduce the number of small patches of incorrectly classified pixels (considered noise). The sieve filter removes all pixel groups smaller than a specified size (threshold), replacing them with their largest neighbouring class. Two filters were applied, one considering the neighbourhood of the 4 pixels on the edges of the selected pixel, and another considering the neighbourhood of the 8 pixels connected to the edges and vertices of the selected pixel. Progressively larger areas were considered, removing polygons of increasing (doubling) size at every interaction (1, 2, 4, 8, 16, . . . , 2048) until the accuracy of the classification stopped increasing and started to decrease due to the loss of relevant information. The total cover area of *C. edulis* was then obtained using the land cover classification with the highest *C. edulis* UA and PA, after application and optimisation of the filter.

The total *C. edulis* AGB was estimated based on: (i) the pixels' VI values in the area classified as *C. edulis*; (ii) the regression model correlating the VI value with the DW of the AGB of *C. edulis*; (iii) the relationship between the DW and WW; and (iv) the ratio between the WW of the green and brown parts of the plants. For the biomass estimation, each *C. edulis*

pixel VI value was converted into AGB DW using the regression model. Then, the WW was estimated based on the DW. Finally, the green/brown parts ratio was used to add an estimate for the AGB of the lower-layer brown parts.

3. Results

3.1. Surveys and Classification

Six significant classes could be visually identified in the resulting images: Water, Dry Sand, Wet Sand, *C. edulis*, Dry Vegetation, and Green Vegetation. Dry vegetation and Green Vegetation included all the vegetation species found in the area that were not identified as *C. edulis*. The mean spectral signature of each class is shown in Figure 5.

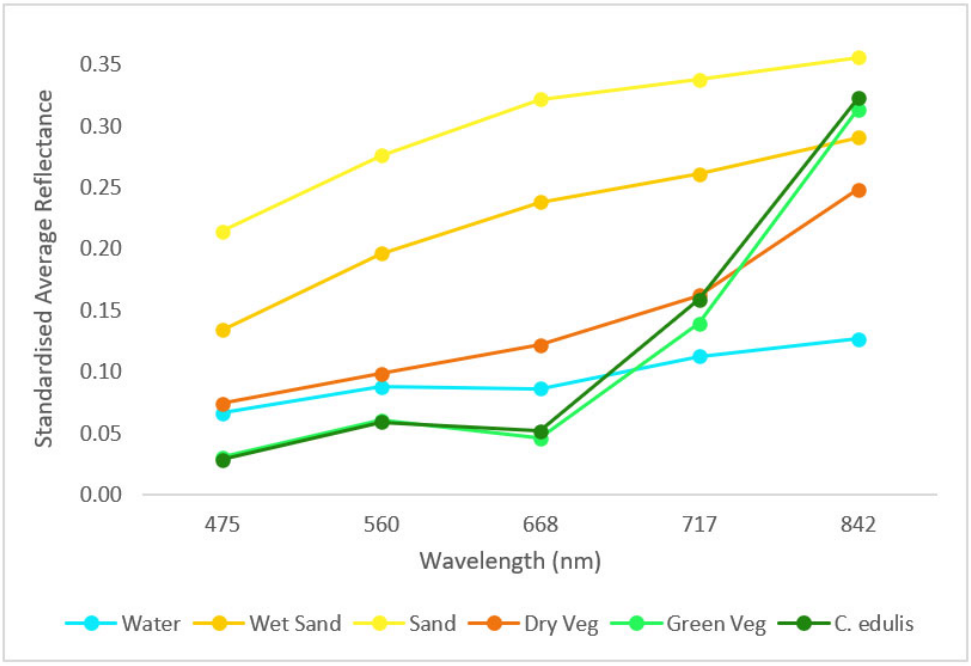

Figure 5. Mean spectral signature of the different classes used in the classification.

The five supervised classification algorithms resulted in different cover classifications, with varying proportions of the target species *C. edulis* (Figure 6).

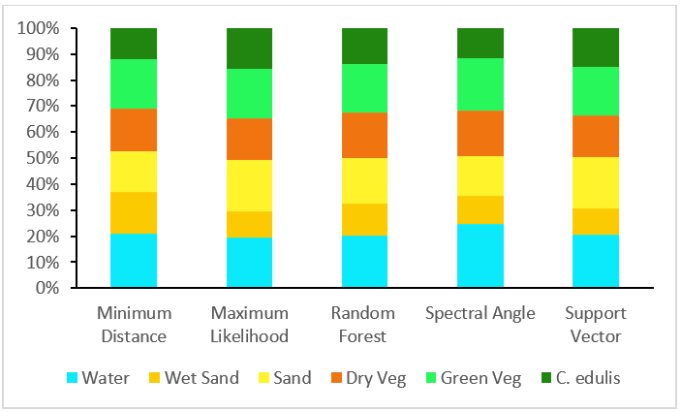

Figure 6. Cover class distribution for each classification algorithm.

According to Equation (1), 600 randomly selected pixels were evaluated for an accuracy assessment, for 518 of which the cover could be clearly identified. The accuracy of each classification is presented on Table 3.

Table 3. Accuracy evaluation of the classification algorithms.

Algorithm	*C. edulis* PA *	*C. edulis* UA *	Kappa	Overall Accuracy
Minimum Distance	0.65	0.72	0.76	0.80
Maximum Likelihood	0.74	0.60	0.80	0.84
Random Forest	0.83	0.73	0.84	0.87
Spectral Angle Mapper	0.79	0.66	0.76	0.77
Support Vector Machine	0.81	0.67	0.82	0.85

* UA—User Accuracy; PA—Producer Accuracy.

The Random Forest algorithm achieved higher overall accuracy, Kappa, and *C. edulis* UA and PA values and was selected for post-processing.

In the post-processing procedure, the use of the sieve filters showed a continuous improvement in classification User's and Producer's accuracy, up to a threshold of 512 pixels. After this, accuracy dropped, suggesting a loss of information (Figures 7 and 8).

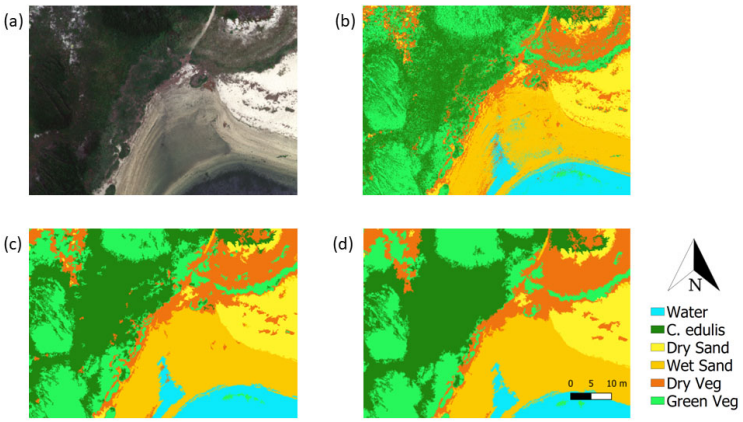

Figure 7. Section of the RGB orthomosaic (**a**), of the Random Forest classification after application of a sieve filter with a threshold = 2 (**b**), a threshold = 512 (**c**), and a threshold = 2048 (**d**).

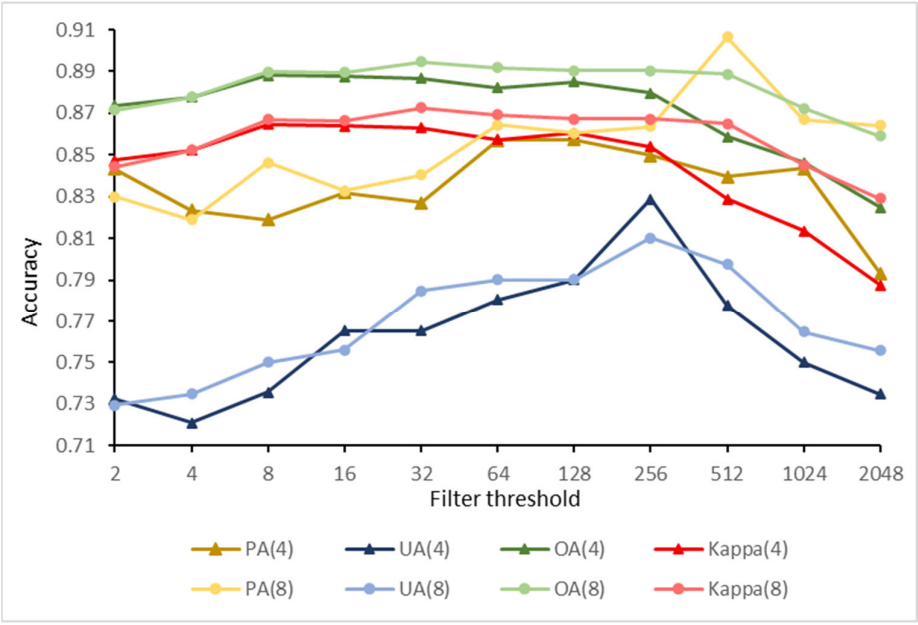

Figure 8. Accuracy measures (PA: Producer Accuracy, UA: User Accuracy, OA: Overall Accuracy) for the Random Forest classification results after the application of sieve filters with increasing thresholds, using a 4 or 8-pixel neighbourhood (between brackets).

The *C. edulis* cover area was estimated using the classification filtered with a 512 threshold and a connectedness of eight squares. According to the classification, 3821 m^2—i.e., about 12%—of the study area was covered with *C. edulis*; on the reference raster, the estimated *C. edulis* cover area was 3362 ± 219 m^2. The detailed classification results are presented in Table 4.

Table 4. Area-based classification error matrix.

		Reference							
		Water	***C. edulis***	**Sand**	**Wet Sand**	**Dry Vegetation**	**Green Vegetation**	**% Area**	**Total Area m^2**
Classified	Water	0.198	0.000	0.000	0.005	0.000	0.002	20.5	6300
	C. edulis	0.000	0.099	0.000	0.000	0.004	0.021	12.4	3821
	Sand	0.000	0.002	0.164	0.006	0.009	0.000	18.1	5565
	Wet Sand	0.005	0.000	0.003	0.097	0.002	0.000	10.7	3279
	Dry Vegetation	0.000	0.002	0.015	0.006	0.163	0.017	20.3	6242
	Green Vegetation	0.000	0.006	0.000	0.000	0.006	0.168	18.0	5540
	% Area	20.3	10.9	18.2	11.4	18.5	20.8	100	
	Total Area m^2	6232	3362	5596	3497	5673	6387		30,748
	Standard Error m^2	148	219	245	214	319	290		
	Producer Accuracy	0.98	0.91	0.90	0.85	0.88	0.81		
	User Accuracy	0.97	0.80	0.91	0.91	0.80	0.93		

3.2. Biomass Estimation

Sample wet and dry weights for the green and brown parts of the collected *C. edulis* plants are presented in Table 5.

Table 5. Summary statistics of *C. edulis* sample wet weights and dry weights for the plants' green and brown parts.

	Green		**Brown**	
	WW (g/m^2)	**DW (g/m^2)**	**WW (g/m^2)**	**DW (g/m^2)**
Maximum	27,120	2860	3650	2637
Minimum	1781	421	117	60
Mean	8912	1188	1093	680
Median	8035	1034	642	370
SD	6175	657	1052	687

To estimate the proportions of the WW of the Green (WW_{green}) and Brown plant parts (WW_{brown}), a simple average ratio was calculated using all the samples—being the mean ratio WW_{green}/WW_{brown} = 15.9. The relationship between the WW and DW of the Green parts was clearly linear, with a mean ratio WW_{green}/DW_{green} = 7.0.

The relationships between the sample's DW and the sample area mean values for the 16 VIs are presented in Table 6. For each VI, the best DW_{green}—VI regression model is shown. Regression models for the DW of the brown parts were not significant for any of the indices (p-values > 0.05) All DW_{green}—VI regressions were significant (p-value < 0.05), except CVI (p-value = 0.3183).

Table 6. Ranking of the best DW_{green}—VI regression models for each VI, with respective R^2 and model type.

Ranking	VI	R^2	Model
1	RDVI	0.86	$y = ab^x$
2	GDVI	0.84	$y = ae^{xb}$
3	DVI	0.84	$y = ae^{xb}$
9	RVI	0.81	$y = ae^{xb}$
10	GCI	0.80	$y = ae^{xb}$
11	ENDVI	0.80	$y = ab^x$
12	NDVI	0.79	$y = ab^x$
13	PRI	0.79	$y = ab^x$
14	GNDVI	0.78	$y = ab^x$
22	MGRVI	0.72	$y = ab^x$
23	ARVI	0.71	$y = ab^x$
25	ExR	0.70	$y = ab^x$
33	RB	0.62	$y = ae^{xb}$
34	ExG	0.62	$y = ab^x$
36	NDREI	0.59	$y = ab^x$
46	CVI	0.00	$y = a + bx$

The Renormalized Difference Vegetation Index (RDVI) presented the best relationship between the samples' DW_{green} and the mean VI value for the sample areas (Figure 9). The RDVI was therefore used to estimate the total *C. edulis* biomass in the study area, computing the DW_{green} for all pixels classified as *C. edulis*.

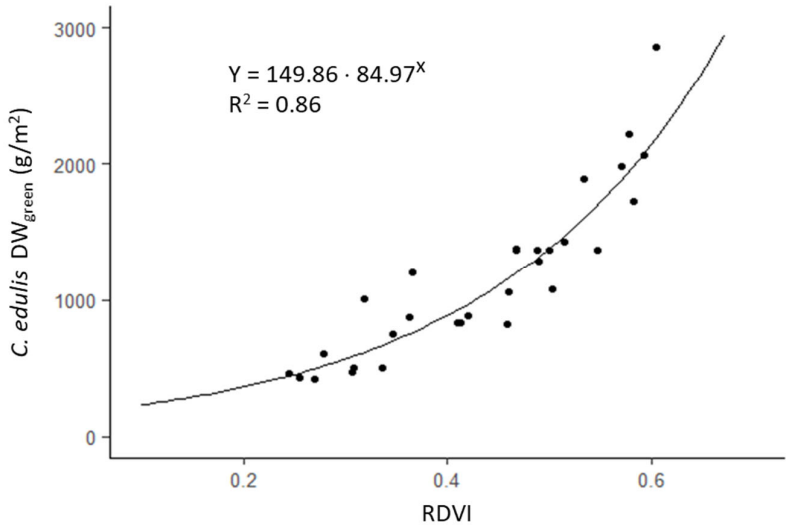

Figure 9. The best-fitting regression model for the sample quadrats' green AGB DW based on the RDVI.

Application of the regression model to the 3821 m^2 of *C. edulis* resulted in an estimated 4431 kg of DW_{green}. Then, this value was converted to WW_{green} using the above-mentioned WW/DW ratio of 7.0, resulting in 31,313 kg of WW_{green}. Finally, the total AGB of *C. edulis* in the area was estimated using the WW_{green}/WW_{brown} ratio of 15.9, which resulted in 32,967 kg of aerial parts of the invasive species in the study area, corresponding to an average AGB of 8.6 kg/m^2 of *C. edulis cover*.

4. Discussion

The use of multispectral UAS for identifying and monitoring invasive species is a well-known technique that has been evaluated for different species and ecosystems [42–45]. Besides this, UAS have also played an important role in commercial crop yield estimation [46–49]. More

recent studies have successfully integrated species identification with yield estimations to assess the Above-Ground Biomass (AGB) of vegetation using multi/hyperspectral UAS [50,51].

In this study, the identification of *C. edulis* through supervised classification of multispectral UAS imagery produced a satisfactory result (*C. edulis* PA = 0.91 *C. edulis* UA = 0.80, kappa = 0.87, OA = 0.89—see Table 4) if compared to similar studies [52–54]. The extra red-edge and near-infrared bands (next to the standard red, green, and blue) of the multispectral imagery allow a better classification and the calculation of VIs that can be used to assess vegetation traits, condition, and biomass [13,55,56]. This is evident in Figure 4, where—even though the mean spectral signatures for the classes *C. edulis* and "green vegetation" present some overlap, especially in the visible spectrum—the red-edge and near-infrared bands are sufficiently distinct to clearly discriminate between these two (see Table 4).

For the estimation of the plant biomass, the RDVI performed best. The regression model of the mean RDVI and DW_{green} provided a satisfactory result (R^2 = 0.86, *p*-value < 0.05, NRMSE = 0.09). Many studies have achieved promising results using the NDVI to evaluate different quantifiable vegetation attributes [57–61]. As a result, NDVI has become the dominant index for vegetation research [62]. However, in this study, NDVI only ranked as the seventh-best model for DW prediction (Table 6). This result is in line with other findings that suggest that different VIs may present a better correlation with vegetation AGB or other attributes than the commonly used NDVI [58], depending on the specific research subject and conditions. Developing a specific methodology to test the accuracy of different VIs as predictors of vegetation attributes is a topic that still needs research and must cover a wide range of variables such as species, surrounding terrain, and weather and light conditions [55]. Furthermore, the morphology variability of vegetation species in nature poses an additional challenge for finding a universal correlation between image data and quantifiable attributes of vegetation species in general. Consequently, a possible correlation between plant AGB and VI must be investigated case by case [58].

Even though this study achieved a good result for the prediction of DW_{green} using VIs, some uncertainties are associated with calculating the total AGB. Next to the well-known classification and regression model uncertainties, it is crucial to also consider other uncertainties that could not be quantified. For example, the WW–DW ratio has a linear correlation, and a mean ratio can be considered a good approximation. Still, this involves many variables that change spatially and temporally. For example, some plants might be in more humid places than others and be in different life stages, which may change the ratio.

An even more accentuated uncertainty was specific to the morphology of *C. edulis*, which develops two layers: an upper succulent green layer and a drier brown layer. This particularity can be a challenge for estimating the AGB for a generic location based on a model. There was no clear relationship between DW_{green} and DW_{brown} and all regression models presented a *p*-value > 0.05, so a simple average was used as the best possible estimate of the ratio between layers; besides, it is possible to conjecture that this ratio can be affected by many variables, such as plant age, growth rate, decay velocity, seasonality, and water and light availability. The distinction between vegetation covers may be more or less successful depending on the season and state of the plants, and the spectral signatures are likely not completely transferable from one season to another or even from one region to another. In the present work, the survey took place in spring, before flowering—as flowers were thought to negatively affect classification results and biomass estimation through VIs. However, a recent study by Innangi, M. et al. [63] that classified *C. edulis* during the flowering season showed that flowers do not have a significant impact on image classification.

Estimating the AGB of *C. edulis* plays an important role in invasive species control, as the estimated biomass serves as an input for planning and implementing removal campaigns. However, the methodology applied in this study can also be used to estimate other plant species' AGB and even to estimate the total carbon content in habitats with a given biomass–carbon correlation. Furthermore, it would be interesting to investigate the possibility of creating a general model for *C. edulis* VI–DW prediction. Therefore, many additional tests would need to be performed to evaluate possible patterns relating VIs with AGB, using the

same methodology as in the present study. Further investigations could also address the use of VIs to optimize land cover classifications, assessing the capability of VIs to provide a better identification of *C. edulis*. Other relevant research might include the applicability and accuracy of this methodology using imagery with lower resolutions, such as aerial photography from planes or satellite images, to monitor *C. edulis*' distribution and biomass.

Finally, it is interesting to notice that the same UAS multispectral images used to monitor *C. edulis* in this study can also provide valuable information for other coastal environment monitoring, such as coastal dune evolution/erosion [64], different vegetation species monitoring [65], and litter mapping and identification [66,67]. The possibility of the multipurpose use of UAS data can optimize data acquisition and, sometimes, provide synergies for different investigations using remote sensing multispectral tools.

5. Conclusions

The present study showed the possibility of using VIs to estimate the AGB of *C. edulis* based on high-resolution multispectral images to monitor this invasive species' dispersion and level of intrusion in coastal sand dunes. Even though some uncertainties linked to this specific species' morphology have to be considered, the methodology can provide valid estimates of its degree of invasion and, consequently, indicates the amount of work necessary to remove the invasive species from an invaded area.

Of the sixteen VIs evaluated, the RDVI presented the best correlation with DW in this study. Considering the many differences between plant species, VI–DW models should be investigated case by case, to understand the individual relationships and find the most suitable model and VI for each specific species.

Author Contributions: Conceptualization, M.d.F.M., J.F.R.C., S.C.d.C.e.S.R. and A.M.F.B.; Methodology, M.d.F.M., J.F.R.C., S.C.d.C.e.S.R. and A.M.F.B.; Software, M.d.F.M., J.A.G., J.F.R.C. and A.M.F.B.; Validation, J.A.G. and A.M.F.B.; Formal analysis, J.F.R.C., S.C.d.C.e.S.R. and A.M.F.B.; Investigation, M.d.F.M.; Resources, J.A.G. and A.M.F.B.; Data curation, M.d.F.M. and J.A.G.; Writing—original draft, M.d.F.M. and A.M.F.B.; Writing—review & editing, J.F.R.C., J.A.G., S.C.d.C.e.S.R. and A.M.F.B.; Visualization, M.d.F.M.; Supervision, J.A.G. and A.M.F.B.; Project administration, A.M.F.B.; Funding acquisition, A.M.F.B. All authors have read and agreed to the published version of the manuscript.

Funding: This research was partially funded by the Ocean3R (NORTE-01-0145-FEDER-000064) and ATLANTIDA (NORTE-01-0145-FEDER-000040) projects, supported by the Norte Portugal Regional Operational Programme (NORTE 2020) under the PORTUGAL 2020 Partnership Agreement, and supported by national funds through FCT—Foundation for Science and Technology within the scope of UIDB/04423/2020 and UIDP/04423/2020. FCT further contributed with a Ph.D. fellowship awarded to J. Cunha (PD/BD/150359/2019) and a contract to S. Ramos (DL 57/2016/CP1344/CT0020).

Institutional Review Board Statement: Not applicable.

Informed Consent Statement: Not applicable.

Data Availability Statement: The datasets analysed will be made available (upon request) through the institution's geographic data server (https://gis.ciimar.up.pt).

Conflicts of Interest: The authors declare no conflict of interest. The funders had no role in the design of the study; in the collection, analyses, or interpretation of data; in the writing of the manuscript; or in the decision to publish the results.

References

1. Rodríguez-Revelo, N.; Espejel, I.; García, C.A.; Ojeda-Revah, L.; Vázquez, M.A.S. Environmental Services of Beaches and Coastal Sand Dunes as a Tool for Their Conservation. In *Beach Management Tools—Concepts, Methodologies and Case Studies*; Botero, C.M., Cervantes, O., Finkl, C.W., Eds.; Coastal Research Library; Springer International Publishing: Cham, Switzerland, 2018; Volume 24, pp. 75–100. ISBN 978-3-319-58303-7.
2. Calvão, T.; Pessoa, M.F.; Lidon, M. Impact of Human Activities on Coastal Vegetation? A Review. *Emir. J. Food Agric* **2013**, *25*, 926. [CrossRef]

3. Feagin, R.A.; Furman, M.; Salgado, K.; Martinez, M.L.; Innocenti, R.A.; Eubanks, K.; Figlus, J.; Huff, T.P.; Sigren, J.; Silva, R. The Role of Beach and Sand Dune Vegetation in Mediating Wave Run up Erosion. *Estuar. Coast. Shelf Sci.* **2019**, *219*, 97–106. [CrossRef]
4. Say, S.E.; Py, K. Implications of Sea Level Rise for Coastal Dune Habitat Conservation in Wales, UK. *J. Coast. Conser.* **2007**, *11*, 31–52. [CrossRef]
5. Giulio, S.; Acosta, A.T.R.; Carboni, M.; Campos, J.A.; Chytrý, M.; Loidi, J.; Pergl, J.; Pyšek, P.; Isermann, M.; Janssen, J.A.M.; et al. Alien Flora across European Coastal Dunes. *Appl. Veg. Sci.* **2020**, *23*, 317–327. [CrossRef]
6. Campoy, J.G.; Acosta, A.T.R.; Affre, L.; Barreiro, R.; Brundu, G.; Buisson, E.; González, L.; Lema, M.; Novoa, A.; Retuerto, R.; et al. Monographs of Invasive Plants in Europe: *Carpobrotus*. *Bot. Lett.* **2018**, *165*, 440–475. [CrossRef]
7. Conser, C.; Connor, E.F. Assessing the Residual Effects of Carpobrotus Edulis Invasion, Implications for Restoration. *Biol. Invasions* **2009**, *11*, 349–358. [CrossRef]
8. Molinari, N.; D'Antonio, C.; Thomson, G. 7 Carpobrotus as a Case Study of the Complexities of Species Impacts. In *Theoretical Ecology Series*; Elsevier: Amsterdam, The Netherlands, 2007; Volume 4, pp. 139–162. ISBN 978-0-12-373857-8.
9. Vieites-Blanco, C.; González-Prieto, S.J. Effects of Carpobrotus Edulis Invasion on Soil Gross N Fluxes in Rocky Coastal Habitats. *Sci. Total Environ.* **2018**, *619–620*, 966–976. [CrossRef]
10. Laporte-Fauret, Q.; Lubac, B.; Castelle, B.; Michalet, R.; Marieu, V.; Bombrun, L.; Launeau, P.; Giraud, M.; Normandin, C.; Rosebery, D. Classification of Atlantic Coastal Sand Dune Vegetation Using In Situ, UAV, and Airborne Hyperspectral Data. *Remote Sens.* **2020**, *12*, 2222. [CrossRef]
11. Yang, C. A High-Resolution Airborne Four-Camera Imaging System for Agricultural Remote Sensing. *Comput. Electron. Agric.* **2012**, *88*, 13–24. [CrossRef]
12. Magney, T.S.; Eitel, J.U.H.; Huggins, D.R.; Vierling, L.A. Proximal NDVI Derived Phenology Improves In-Season Predictions of Wheat Quantity and Quality. *Agric. For. Meteorol.* **2016**, *217*, 46–60. [CrossRef]
13. Jang, G.; Kim, J.; Yu, J.-K.; Kim, H.-J.; Kim, Y.-H.; Kim, D.-W.; Kim, K.-H.; Lee, C.; Chung, Y.S. Review: Cost-Effective Unmanned Aerial Vehicle (UAV) Platform for Field Plant Breeding Application. *Remote Sens.* **2020**, *12*, 998. [CrossRef]
14. Baena, S.; Moat, J.; Whaley, O.; Boyd, D.S. Identifying Species from the Air: UAVs and the Very High Resolution Challenge for Plant Conservation. *PLoS ONE* **2017**, *12*, e0188714. [CrossRef]
15. Alvarez-Taboada, F.; Paredes, C.; Julián-Pelaz, J. Mapping of the Invasive Species Hakea Sericea Using Unmanned Aerial Vehicle (UAV) and WorldView-2 Imagery and an Object-Oriented Approach. *Remote Sens.* **2017**, *9*, 913. [CrossRef]
16. Lopatin, J.; Dolos, K.; Kattenborn, T.; Fassnacht, F.E. How Canopy Shadow Affects Invasive Plant Species Classification in High Spatial Resolution Remote Sensing. *Remote. Sens. Ecol. Conserv.* **2019**, *5*, 302–317. [CrossRef]
17. Liang, W.; Abidi, M.; Carrasco, L.; McNelis, J.; Tran, L.; Li, Y.; Grant, J. Mapping Vegetation at Species Level with High-Resolution Multispectral and Lidar Data Over a Large Spatial Area: A Case Study with Kudzu. *Remote Sens.* **2020**, *12*, 609. [CrossRef]
18. Koco, Š.; Dubravská, A.; Vilček, J.; Gruľová, D. Geospatial Approaches to Monitoring the Spread of Invasive Species of *Solidago* Spp. *Remote Sens.* **2021**, *13*, 4787. [CrossRef]
19. Baloloy, A.B.; Blanco, A.C.; Candido, C.G.; Argamosa, R.J.L.; Dumalag, J.B.L.C.; Dimapilis, L.L.C.; Paringit, E.C. Estimation of mangrove forest aboveground biomass using multispectral bands, vegetation indices and biophysical variables derived from optical satellite imageries: Rapideye, planetscope and sentinel-2. *ISPRS Ann. Photogramm. Remote Sens. Spatial Inf. Sci.* **2018**, *4*, 29–36. [CrossRef]
20. Al-lami, A.K.; Abbood, R.A.; Al Maliki, A.A.; Al-Ansari, N. Using Vegetation Indices for Monitoring the Spread of Nile Rose Plant in the Tigris River within Wasit Province, Iraq. *Remote Sens. Appl. Soc. Environ.* **2021**, *22*, 100471. [CrossRef]
21. Brown, S.; Narine, L.L.; Gilbert, J. Using Airborne Lidar, Multispectral Imagery, and Field Inventory Data to Estimate Basal Area, Volume, and Aboveground Biomass in Heterogeneous Mixed Species Forests: A Case Study in Southern Alabama. *Remote Sens.* **2022**, *14*, 2708. [CrossRef]
22. Gomes, P.T.; Botelho, A.A.; Soares de Carvalho, G. *Sistemas dunares do litoral de Esposende*; Universidade do Minho: Braga, Portugal, 2002; ISBN 978-972-9027-16-1.
23. Carvalho, G.S.; Granja, H.; Gomes, P.; Loureiro, E.; Renato, H.; Ribeiro, I.; Costa, A.L. New Data and New Ideas Concerning Recent Geomorphological Changes in the NW Coastal Zone of Portugal. In Proceedings of the Littoral 2002: 6th International Symposium: The Changing Coast, Porto, Portugal, 22–26 September 2002.
24. Kaufman, Y.J.; Tanre, D. Atmospherically Resistant Vegetation Index (ARVI) for EOS-MODIS. *IEEE Trans. Geosci. Remote Sensing* **1992**, *30*, 261–270. [CrossRef]
25. Gitelson, A.A. Remote Estimation of Canopy Chlorophyll Content in Crops. *Geophys. Res. Lett.* **2005**, *32*, L08403. [CrossRef]
26. Vincini, M.; Frazzi, E.; D'Alessio, P. A Broad-Band Leaf Chlorophyll Vegetation Index at the Canopy Scale. *Precis. Agric* **2008**, *9*, 303–319. [CrossRef]
27. Richardson, A.D.; Duigan, S.P.; Berlyn, G.P. An Evaluation of Noninvasive Methods to Estimate Foliar Chlorophyll Content. *New Phytol.* **2002**, *153*, 185–194. [CrossRef]
28. Rasmussen, J.; Ntakos, G.; Nielsen, J.; Svensgaard, J.; Poulsen, R.N.; Christensen, S. Are Vegetation Indices Derived from Consumer-Grade Cameras Mounted on UAVs Sufficiently Reliable for Assessing Experimental Plots? *Eur. J. Agron.* **2016**, *74*, 75–92. [CrossRef]
29. Rouse, J.W.; Haas, R.H.; Deering, D.W.; Schell, J.A.; Harlan, J.C. *Monitoring the Vernal Advancement and Retrogradation (Green Wave Effect) of Natural Vegetation*; Great Plains Corridor; NASA: Greenbelt, MD, USA, 1973.

30. Meyer, G.E.; Neto, J.C. Verification of Color Vegetation Indices for Automated Crop Imaging Applications. *Comput. Electron. Agric.* **2008**, *63*, 282–293. [CrossRef]
31. Gitelson, A.A.; Kaufman, Y.J.; Merzlyak, M.N. Use of a Green Channel in Remote Sensing of Global Vegetation from EOS-MODIS. *Remote Sens. Environ.* **1996**, *58*, 289–298. [CrossRef]
32. Bendig, J.; Yu, K.; Aasen, H.; Bolten, A.; Bennertz, S.; Broscheit, J.; Gnyp, M.L.; Bareth, G. Combining UAV-Based Plant Height from Crop Surface Models, Visible, and near Infrared Vegetation Indices for Biomass Monitoring in Barley. *Int. J. Appl. Earth Obs. Geoinf.* **2015**, *39*, 79–87. [CrossRef]
33. Gitelson, A.; Merzlyak, M.N. Quantitative Estimation of Chlorophyll-a Using Reflectance Spectra: Experiments with Autumn Chestnut and Maple Leaves. *J. Photochem. Photobiol. B Biol.* **1994**, *22*, 247–252. [CrossRef]
34. Gamon, J.A.; Peñuelas, J.; Field, C.B. A Narrow-Waveband Spectral Index That Tracks Diurnal Changes in Photosynthetic Efficiency. *Remote Sens. Environ.* **1992**, *41*, 35–44. [CrossRef]
35. Roujean, J.-L.; Breon, F.-M. Estimating PAR Absorbed by Vegetation from Bidirectional Reflectance Measurements. *Remote Sens. Environ.* **1995**, *51*, 375–384. [CrossRef]
36. Pearson, R.L.; Miller, L.D. Remote Mapping of Standing Crop Biomass for Estimation of the Productivity of the Shortgrass Prairie, Pawnee National Grasslands, Colorado. IBP Grassland Biome; Department of Watershed Sciences, College of Forestry and Natural Resources, Colorado State University: Fort Collins, CO, USA, 1972.
37. Richards, J.A. *Remote Sensing Digital Image Analysis: An Introduction*; Springer: Berlin/Heidelberg, Germany, 2013; ISBN 978-3-642-30061-5.
38. Kruse, F.A.; Lefkoff, A.B.; Boardman, J.W.; Heidebrecht, K.B.; Shapiro, A.T.; Barloon, P.J.; Goetz, A.F.H. The Spectral Image Processing System (SIPS)—Interactive Visualization and Analysis of Imaging Spectrometer Data. *Remote Sens. Environ.* **1993**, *44*, 145–163. [CrossRef]
39. Boser, B.E.; Guyon, I.M.; Vapnik, V.N. A Training Algorithm for Optimal Margin Classifiers. In Proceedings of the Fifth Annual Workshop on Computational Learning Theory, Pittsburgh, PA, USA, 27–29 July 1992; ACM: Pittsburgh, PA, USA, July, 1992; pp. 144–152.
40. Ho, T.K. Random Decision Forests. In Proceedings of the 3rd International Conference on Document Analysis and Recognition, Montreal, QC, Canada, 14–15 August 1995; IEEE Computer Society Press: Montreal, QC, Canada, 1995; Volume 1, pp. 278–282.
41. Olofsson, P.; Foody, G.M.; Herold, M.; Stehman, S.V.; Woodcock, C.E.; Wulder, M.A. Good Practices for Estimating Area and Assessing Accuracy of Land Change. *Remote Sens. Environ.* **2014**, *148*, 42–57. [CrossRef]
42. Gonçalves, C.; Santana, P.; Brandão, T.; Guedes, M. Automatic Detection of Acacia Longifolia Invasive Species Based on UAV-Acquired Aerial Imagery. *Inf. Process. Agric.* **2022**, *9*, 276–287. [CrossRef]
43. Jianhui, L.; Dingquan, L.; Gui, Z.; Haizhou, X.; Rongliang, Z.; Wangjun, L.; Youliang, Y. Study on Extraction of Foreign Invasive Species Mikania Micrantha Based on Unmanned Aerial Vehicle (UAV) Hyperspectral Remote Sensing. In *Proceedings of the Fifth Symposium on Novel Optoelectronic Detection Technology and Application, Xi'an, China, 24–26 October 2018*; Yu, Q., Huang, W., He, Y., Eds.; SPIE: Xi'an, China, 2019; p. 53.
44. Abeysinghe, T.; Simic Milas, A.; Arend, K.; Hohman, B.; Reil, P.; Gregory, A.; Vázquez-Ortega, A. Mapping Invasive Phragmites Australis in the Old Woman Creek Estuary Using UAV Remote Sensing and Machine Learning Classifiers. *Remote Sens.* **2019**, *11*, 1380. [CrossRef]
45. Mallmann, C.L.; Zaninni, A.F.; Filho, W.P. Vegetation Index Based in Unmanned Aerial Vehicle (Uav) to Improve the Management of Invasive Plants in Protected Areas, Southern Brazil. In Proceedings of the 2020 IEEE Latin American GRSS & ISPRS Remote Sensing Conference (LAGIRS), Santiago, Chile, 22–26 March 2020; IEEE: Santiago, Chile, March, 2020; pp. 66–69.
46. Santos, L.M.; Ferraz, G.A.S.; Diotto, A.V.; Barbosa, B.D.S.; Maciel, D.T.; Andrade, M.T.; Ferraz, P.F.P.; Rossi, G. Coffee Crop Coefficient Prediction as a Function of Biophysical Variables Identified from RGB UAS Images. *Agron. Res.* **2020**, *18*, 1463–1471. [CrossRef]
47. Yang, S.; Hu, L.; Wu, H.; Ren, H.; Qiao, H.; Li, P.; Fan, W. Integration of Crop Growth Model and Random Forest for Winter Wheat Yield Estimation from UAV Hyperspectral Imagery. *IEEE J. Sel. Top. Appl. Earth Obs. Remote Sens.* **2021**, *14*, 6253–6269. [CrossRef]
48. Li, B.; Xu, X.; Zhang, L.; Han, J.; Bian, C.; Li, G.; Liu, J.; Jin, L. Above-Ground Biomass Estimation and Yield Prediction in Potato by Using UAV-Based RGB and Hyperspectral Imaging. *ISPRS J. Photogramm. Remote Sens.* **2020**, *162*, 161–172. [CrossRef]
49. Bian, C.; Shi, H.; Wu, S.; Zhang, K.; Wei, M.; Zhao, Y.; Sun, Y.; Zhuang, H.; Zhang, X.; Chen, S. Prediction of Field-Scale Wheat Yield Using Machine Learning Method and Multi-Spectral UAV Data. *Remote Sens.* **2022**, *14*, 1474. [CrossRef]
50. Wengert, M.; Wijesingha, J.; Schulze-Brüninghoff, D.; Wachendorf, M.; Astor, T. Multisite and Multitemporal Grassland Yield Estimation Using UAV-Borne Hyperspectral Data. *Remote Sens.* **2022**, *14*, 2068. [CrossRef]
51. Wijesingha, J.; Astor, T.; Schulze-Brüninghoff, D.; Wachendorf, M. Mapping Invasive Lupinus Polyphyllus Lindl. in Semi-Natural Grasslands Using Object-Based Image Analysis of UAV-Borne Images. *PFG* **2020**, *88*, 391–406. [CrossRef]
52. Michez, A.; Piégay, H.; Jonathan, L.; Claessens, H.; Lejeune, P. Mapping of Riparian Invasive Species with Supervised Classification of Unmanned Aerial System (UAS) Imagery. *Int. J. Appl. Earth Obs. Geoinf.* **2016**, *44*, 88–94. [CrossRef]
53. Papp, L.; van Leeuwen, B.; Szilassi, P.; Tobak, Z.; Szatmári, J.; Árvai, M.; Mészáros, J.; Pásztor, L. Monitoring Invasive Plant Species Using Hyperspectral Remote Sensing Data. *Land* **2021**, *10*, 29. [CrossRef]
54. Sabat-Tomala, A.; Raczko, E.; Zagajewski, B. Comparison of Support Vector Machine and Random Forest Algorithms for Invasive and Expansive Species Classification Using Airborne Hyperspectral Data. *Remote Sens.* **2020**, *12*, 516. [CrossRef]

55. Xue, J.; Su, B. Significant Remote Sensing Vegetation Indices: A Review of Developments and Applications. *J. Sens.* **2017**, *2017*, 1–17. [CrossRef]
56. Gao, L.; Wang, X.; Johnson, B.A.; Tian, Q.; Wang, Y.; Verrelst, J.; Mu, X.; Gu, X. Remote Sensing Algorithms for Estimation of Fractional Vegetation Cover Using Pure Vegetation Index Values: A Review. *ISPRS J. Photogramm. Remote Sens.* **2020**, *159*, 364–377. [CrossRef]
57. Pandey, P.C.; Anand, A.; Srivastava, P.K. Spatial Distribution of Mangrove Forest Species and Biomass Assessment Using Field Inventory and Earth Observation Hyperspectral Data. *Biodivers Conserv.* **2019**, *28*, 2143–2162. [CrossRef]
58. Huang, S.; Tang, L.; Hupy, J.P.; Wang, Y.; Shao, G. A Commentary Review on the Use of Normalized Difference Vegetation Index (NDVI) in the Era of Popular Remote Sensing. *J. For. Res.* **2021**, *32*, 1–6. [CrossRef]
59. Hassan, M.A.; Yang, M.; Rasheed, A.; Yang, G.; Reynolds, M.; Xia, X.; Xiao, Y.; He, Z. A Rapid Monitoring of NDVI across the Wheat Growth Cycle for Grain Yield Prediction Using a Multi-Spectral UAV Platform. *Plant Sci.* **2019**, *282*, 95–103. [CrossRef]
60. Guan, S.; Fukami, K.; Matsunaka, H.; Okami, M.; Tanaka, R.; Nakano, H.; Sakai, T.; Nakano, K.; Ohdan, H.; Takahashi, K. Assessing Correlation of High-Resolution NDVI with Fertilizer Application Level and Yield of Rice and Wheat Crops Using Small UAVs. *Remote Sens.* **2019**, *11*, 112. [CrossRef]
61. Tenreiro, T.R.; García-Vila, M.; Gómez, J.A.; Jiménez-Berni, J.A.; Fereres, E. Using NDVI for the Assessment of Canopy Cover in Agricultural Crops within Modelling Research. *Comput. Electron. Agric.* **2021**, *182*, 106038. [CrossRef]
62. Xu, Y.; Yang, Y.; Chen, X.; Liu, Y. Bibliometric Analysis of Global NDVI Research Trends from 1985 to 2021. *Remote Sens.* **2022**, *14*, 3967. [CrossRef]
63. Innangi, M.; Marzialetti, F.; Di Febbraro, M.; Acosta, A.T.R.; De Simone, W.; Frate, L.; Finizio, M.; Villalobos Perna, P.; Carranza, M.L. Coastal Dune Invaders: Integrative Mapping of Carpobrotus Sp. Pl. (Aizoaceae) Using UAVs. *Remote Sens.* **2023**, *15*, 503. [CrossRef]
64. Laporte-Fauret, Q.; Marieu, V.; Castelle, B.; Michalet, R.; Bujan, S.; Rosebery, D. Low-Cost UAV for High-Resolution and Large-Scale Coastal Dune Change Monitoring Using Photogrammetry. *JMSE* **2019**, *7*, 63. [CrossRef]
65. Suo, C.; McGovern, E.; Gilmer, A. Coastal Dune Vegetation Mapping Using a Multispectral Sensor Mounted on an UAS. *Remote Sens.* **2019**, *11*, 1814. [CrossRef]
66. Gonçalves, G.; Andriolo, U.; Gonçalves, L.M.S.; Sobral, P.; Bessa, F. Beach Litter Survey by Drones: Mini-Review and Discussion of a Potential Standardization. *Environ. Pollut.* **2022**, *315*, 120370. [CrossRef]
67. Gonçalves, G.; Andriolo, U. Operational Use of Multispectral Images for Macro-Litter Mapping and Categorization by Unmanned Aerial Vehicle. *Mar. Pollut. Bull.* **2022**, *176*, 113431. [CrossRef]